ARCHIVES OF TRANSPORT *ISSN (print):* *0866-9546*
Volume 67, Issue 3, 2023 ***e-ISSN (online):*** *2300-8830*
DOI: *10.5604/01.3001.0053.7357*

DETERMINATION OF DYNAMIC PARAMETERS OF A TRAM WHEEL PARTS IN A NUMERICAL AND EXPERIMENTAL MODAL ANALYSIS

Julia MILEWICZ[1], Krzysztof KOŁODZIEJCZAK[2], Tomasz NOWAKOWSKI[3], Grzegorz M. SZYMAŃSKI[4]

[1, 3, 4] Poznan University of Technology, Institute of Transport, Poznań, Poland

[2] Łukasiewicz Research Network – Poznan Institute of Technology, Poznań, Poland

Abstract:

The analysis of dynamic parameters finds effective application in processes related to the assessment of the technical condition of machines. Mass transport vehicles are particularly sensitive to maintaining an appropriate level of traffic safety through relevant design and diagnostics. The combination of numerical and experimental methods increases the efficiency of modal properties investigations, which can be used as diagnostic parameters. During the research, the authors performed a numerical model of a system composed of a rim and an inner disc of a wheel fitted in a Konstal 105Na tram, widely used in many polish cities and frequently subjected to repair and renovation processes. The Time Response analysis in SOLIDWORKS (also called Modal Time History) was then conducted, resulting in obtaining information about object vibration response in time domain to the impulsive excitation at given points. These signals were then processed in MATLAB aiming at determining the frequencies of natural vibration and damping ratios. The processing parameters in MATLAB were corresponding to the analysis settings of the experimental measurement, carried out within the BK Connect environment, with an impact modal hammer and piezoelectric transducers. When analyzing the experimental measurements, the authors applied Fast Fourier Transformation, Frequency Response Function and Complex Mode Indicator Function (the theoretical basis of which and practical sense of application were also presented in the paper). Finally, the results of the experiment were compared with simulation outcomes. This comparison allowed the obtainment of frequency characteristics of the vibration response to the impact and the determination of the dynamic parameters of the actual object. Six frequencies of natural vibrations were determined in the frequency range of 0 to 3000 Hz, as well as their damping ratios and autocorrelation indicators between modes. Similarities and potential sources of differences between the numerical and the experimental results were identified and explained, followed by conclusions on the practical application of the presented research methodology in the industry.

Keywords: *modal analysis, rail vehicles, simulation, modes extraction*

To cite this article:

Milewicz, J., Kołodziejczak, K., Nowakowski, T., Szymański, G.M., (2023). Determination of dynamic parameters of a tram wheel parts in a numerical and experimental modal analysis. Archives of Transport, 67(3), 119-137. DOI: https://doi.org/10.5604/01.3001.0053.7357

Contact:
1) julia.milewicz@doctorate.put.poznan.pl [https://orcid.org/0000-0002-7360-0790] – corresponding author;
2) krzysztof.kolodziejczak@pit.lukasiewicz.gov.pl [https://orcid.org/0000-0001-6879-7130]; 3) tomasz.nowakowski@put.poznan.pl [https://orcid.org/0000-0001-5415-7052]; 4) grzegorz.m.szymanski@put.poznan.pl [https://orcid.org/0000-0002-2784-9149]

1. Introduction

Modal analysis is widely used in the diagnosis of rail vehicle components and subassemblies. It is used for solving time invariant linear equations describing system behavior, which in consequence enables determination and interpretation of dynamic properties. The modal parameters used in the frequency domain are most often the forms of natural vibration and the vibration frequencies and damping corresponding to them. The analysis of the properties of the solid, its mass, stiffness and interactions with the environment allows to determine the resonance conditions and the influence of the created or propagating defects (Harak et al., 2014).

Modal analysis is a system analysis based on the precise measurement of the vibration of an object, excited on an electrodynamic exciter or mechanically using a modal hammer, and allows the determination of the relationship between geometry and material and technical condition on the basis of the values of natural vibration parameters and their form (Klimenda and Soukup, 2017). The system under study must be linear, observable, with small or proportional damping (Niziński and Michalski, 2002). As a result of modal analysis, a mathematical model and description of its dynamic behavior are obtained. The formulated mathematical model is referred to as the modal model of the system, and the feature information is known as its modal characteristics: the set of natural frequencies and their forms and damping ratios.

The general equation describing the system dynamics in time $\mathbf{f}(t)$ was presented below (Van de Aweraer, 2001; Cong et al., 2022):

$$\mathbf{M}\ddot{\mathbf{x}}(t) + \mathbf{C}\dot{\mathbf{x}}(t) + \mathbf{K}\mathbf{x}(t) = \mathbf{f}(t) \tag{1}$$

where **M**, **C** and **K** are respectively the matrices of masses, damping and stiffness ratios. $\mathbf{x}, \dot{\mathbf{x}}, \ddot{\mathbf{x}}$ are vectors, which relate to the displacement, velocity and acceleration, **f***(t)* is the external loading vector.

By using the Fourier transform, when the relations $\mathbf{f}(t) = \mathbf{F}(\omega)e^{j\omega t}$ and $\mathbf{x}(t) = \mathbf{X}(\omega)e^{j\omega t}$ occur, it is possible to describe the dynamics of the system in a frequency-dependent manner (Hassani and Shadan, 2022):

$$(-\omega^2\mathbf{M} + j\omega\mathbf{C} + \mathbf{K})\mathbf{X}(\omega) = \mathbf{F}(\omega) \tag{2}$$

where ω describes the driving frequency, **X(***ω)* the displacement, **F(***ω)* the external force and *j* is an imaginary number equal to $\sqrt{-1}$.

The solution of these equations is possible by obtaining eigenvalues, in the form of modal parameters. For the actual structure, equation (2) can also be expressed as:

$$(-\omega^2\mathbf{M}^* + j\omega\mathbf{C}^* + \mathbf{K}^*)\mathbf{X}^*(\omega) = \mathbf{F}^*(\omega) \tag{3}$$

where $\mathbf{M}^*$, $\mathbf{C}^*$ and $\mathbf{K}^*$ are, respectively, the matrices of masses, damping ratios and stiffness of the actual structure and $\mathbf{X}^*$ corresponds to the actual modal displacement. The solution of this system is accomplished by determining the vibration and eigenvectors. The eigenvectors are expressed through physical coordinate bases on the structure, and correspond to characteristic patterns of structural vibration, referred to as eigenmodes. Each of these forms can be understood as an independent system with one degree of freedom. A detailed description of the theoretical basis of modal testing is presented in (Ewins, 2000).

The modal representation of the system can be determined theoretically: analytically, numerically (using the finite element method) and experimentally. In case of the experimental method, the measurement results are digitally processed using the implementation of automatic by estimation of model parameters.

2. Literature review

Modal analysis can be used both for current diagnosis of objects (e.g. smaller machine components) at the stage of design, prototype and operation, as well as for prediction of potential failures through observation of changes of dynamic parameters under the influence of operating forces. An example of such research in the area of railroads is presented in the paper (Harak and Harsha, 2014). It presents numerical analysis of the model consisting of the freight car body and bogies for the conditions simulating the influence of trackway irregularities, which were the source of vertical vibrations. Operational modal analysis, described in (Teimouri-Sichani and Ahmadian, 2006) allowed, on the other hand, to identify the properties directly related to the suspension or springs of the rail vehicle.

Numerical investigations of modal properties of wheelsets were described in (Sowiński, 2016;

Cataldi et al., 2004) for identification of modes and changes of parameters under the influence of wear. The comparative analysis of wheel construction, with damping and monoblock elements, in the context of vibration effects of the vehicle on its surroundings was also performed (Suarez et al., 2006; Cigada et al., 2008]. The connection between the increase of vibration intensity in certain frequency bands under the influence of simulated operational forces (Cataldi et al., 2004) and the possibility of detecting wear of running surface (Cigada et al., 2008) was proved. None of these studies concerned the object without additional dynamic loads, related to the vehicle motion, and was not coordinated with the realization of the experimental model. Among the experimental methods for the use of vibroacoustic signal analysis in the context of rail vehicle wheel research, the determination of wheel irregularities (Komorski et al., 2018a) and the detection of flat spots on the rolling surface (Komorski et al., 2018b) have already been investigated. Wheels of rail vehicles are a difficult test object because of the complex geometry of the structure and methods of joining elements that impart additional internal stresses. In addition, experimental analysis requires optimal placement of numerous measurement points.

An effective diagnostic tool is to combine numerical analysis and modal experiment and then study the correlation of the results. Tuning the structural model and tracking the changes during operation provides reliable information about the technical condition of the object. The comparative evaluation of theoretical and experimental modal models has been applied to different engineering fields, realized on the example of such objects as support beam (Nadkarni et al., 2021) hemispherical shell, including fluid interaction (Eslaminejad et al., 2021), electric submersible pump (Castillo et al., 2019), cross laminated timber floor (Kawrza et al., 2022) and composite laminates (Pereira et al., 2020), among others.

Although combined numerical and experimental modal analysis is used in the railway industry, e.g. for investigating fatigue failures (Wei et al., 2022), it is more often applied to whole wagons, treated as a multi-body system (Nangolo et al., 2014). More common is the numerical analysis of the structural dynamics of modern steel vehicle body structures (Pothamsetty Rao et al., 2022). This indicates a research gap that concerns the calibration of numerical and experimental analyses of the modal properties of the vehicle components themselves, which could serve to optimize diagnostic, as well as design, processes at the prototype and test stage. Properly carried out experiment involves the overcoming of the difficulty of designing and implementing measurement procedures, as described in (Melero et al., 2022). Simulation tests, by calibrating with the real conditions of the experiment, can support the analysis of the component and facilitate the interpretation of the results or point out unforeseen differences in the structural dynamics behavior of the research object. That is why the realized research was carried out to compare the effectiveness of the simulation and experimental method in identifying the dynamic parameters. Applying the interpretation of the multiple forcing and multiple response method to the identification of the dynamic parameters of the tram wheel components provided relevant information with diagnostic potential. Moreover, they make it possible to calibrate the numerical and actual models and to determine the key methodological elements of the analysis. The study indicated the convergence of the results and the effectiveness of the calibration of the actual and theoretical model.

3. Signal processing and mode extraction

Experimental modal analysis is a two-channel analysis in which both the excitation value and the vibration response are recorded. By using the Fast Fourier Transform (FFT), it is possible to go from a time function, in which measurements are made, to a frequency function (Milewicz et al., 2021). The analysis in the time domain allows to determine the values of the signal, while in the frequency domain the energy of the signal is considered, which is much more useful to describe the phenomena of structural dynamics. Thus, the signal can be analyzed from a different perspective, determining its components and dominant vibration frequencies and, consequently, determining the dynamic parameters of the object (Mokrzan et al., 2021). The Frequency Response Function (FRF) (Cigada et al., 2008), also called the transfer function, which describes the ratio of the spectrum of the output signal, i.e. the vibration response to the excitation, to the spectrum of the input signal, i.e. the hammer force

on the test object, is then applicable. The FRF is a mathematical, signal-independent descriptor of the system, which is defined by the formula:

$$\mathbf{H}(\omega) = \frac{\mathbf{X}(\omega)}{\mathbf{F}(\omega)} \tag{4}$$

where $\mathbf{X}(\omega)$ is the output signal in frequency domain and $\mathbf{F}(\omega)$ is the input signal in frequency domain. Linearity and invariance of the model are assumed in such analyses (Jacobsen, 2018). The FRF matrix is understood as a frequency representation of linear structural dynamics, in which the linear spectra of the input signals are multiplied by the corresponding matrix elements to obtain the linear spectra of the output signals. This creates pairs of input and output values for successive degrees of freedom of the structure (Żółtowski and Napieraj, 2017), which can be expressed in terms of matrix relations:

$$\mathbf{X}(\omega) = \mathbf{H}(\omega)\mathbf{F}(\omega) \tag{5}$$

This transfer function is applicable for both single and multiple excitations, where it is necessary to determine the FRF matrix for each spectral line. Depending on the nature of the noise and disturbance during the measurement, a specific FRF analysis estimator is used to minimize errors. For the case of modal hammer forcing, the $\mathbf{H_I}$ estimator is used for the noise in the output signal (Mitchell, 1982).
The value of the estimator is determined from the relation:

$$\mathbf{H_I}(\omega) = \frac{\mathbf{G_{FX}}(\omega)}{\mathbf{G_{FF}}(\omega)} \tag{6}$$

where $\boldsymbol{G_{FX}(\omega)}$ is the cross-spectral density of the input (excitation) and output (response) signals in the frequency domain, $\boldsymbol{G_{FF}}(\omega)$ is the spectral density of its own input signal (excitation) in the frequency domain. However, in the case of expected noise in the input signal, an estimator is $\mathbf{H_{II}}$ is used, expressed by the formula:

$$\mathbf{H_{II}}(\omega) = \frac{\mathbf{G_{XX}}(\omega)}{\mathbf{G_{FX}}(\omega)} \tag{7}$$

where $\boldsymbol{G}_{\mathbf{XX}}(\omega)$ is the spectral density of its own output signal (response) in the frequency domain and $\boldsymbol{G}_{\mathbf{XX}}(\omega)$ is the cross-spectral density of the input (excitation) and output (response) signals in the frequency domain. When the object meets all assumptions, and noise and measurement errors are not present, these two estimators should be equal to FRF: $\mathbf{H_I}(\omega) = \mathbf{H_{II}}(\omega) = \mathbf{H}(\omega)$. **Hv** estimator is also distinguished, which can be used in the situation of signal interference in both excitation and response measurements.
In addition to using the FRF function, which does not present all the necessary information about the dynamic parameters, the CMIF - Complex Mode Indicator Function method was also used to analyze the results. This method does not require pre-estimation of dynamic parameters and the actual values of modal properties are obtained by acting on matrices.
The method is based on the Singular Value Decomposition (SVD) of the normal matrix, formed from the FRF matrix (Allemang and Brown, 2006; Agneni et al., 2010), for each $[\mathbf{H}(j\omega)]^{\mathrm{H}}[\mathbf{H}(j\omega)]$ spectral line.
The SVD decomposition itself, described e.g. in (Bakir et al., 2010), consists in decomposing a given matrix into the product of two orthogonal matrices and one diagonal matrix, in order to reduce its dimension and determine its recurring values. Then the following relation can be obtained:

$$\mathbf{H}(\omega) = \mathbf{U}(\omega) \sum(\omega)\, \mathbf{V}(\omega)^{\mathrm{H}} \tag{8}$$

where: $\mathbf{U}(\omega)$ and $\mathbf{V}(\omega)$ are unitarity matrices determined by N eigenvectors, differing in size (corresponding to the number of response points and excitation, respectively) and $\sum(\omega)$ is a diagonal unitary matrix corresponding to the number of dominant modes (by "dominant" is meant one that causes the structure to respond at a given frequency (ω)).
The CMIF values are equal to the square of the magnitude of the singular values of the determined matrix, so it is possible to see peaks in the plot of the function in the frequency domain that correspond to the parameters of the eigenvalue vibrations (Hunady & Hagara, 2015):

$$\mathbf{CMIF}_{\mathrm{k}}(\omega) = \boldsymbol{\mu}_{\mathrm{k}}(\omega) = \boldsymbol{\sigma}_{\mathrm{k}}^{2}(\omega) \tag{9}$$

$$\mathbf{H}(\omega)^{\mathrm{H}}\mathbf{H}(\omega) = \mathbf{U}(\omega)\sum{}^{2}(\omega)\mathbf{V}(\omega)^{\mathrm{H}} \tag{10}$$

where $k = 1,2, \ldots, N_r$, $\mathbf{CMIF_k}(\omega)$ is the k[th] CMIF at frequency ω, $\boldsymbol{\mu_k}(\omega)$ is the k[th] eigenvalue of the normal matrix of FRF matrix at frequency ω, $\boldsymbol{\sigma_k}(\omega)$ is the k[th] singular value of the FRF matrix at frequency ω.

In this way, it is possible to identify individual modes, determine their frequencies, form and damping ratios, as well as global modal parameters. Signal filtering, based on principal component decomposition, is also applied in operational modal analysis when measuring the vibrational response to unknown harmonic excitation and disturbances (Amirali and Shapou, 2021).

The Rational Fraction Polynomial-Z method, recommended for systems with many degrees of freedom and small disturbances (Omar et al., 2010), is used for modal estimation. It involves representing the FRF function as a measurable ratio of two polynomials such that the numerator and denominator values are of independent orders. This action can be represented in the form of equation:

$$\mathbf{H}(\omega) = \frac{\sum_{k=0}^{m} a_k(\omega)^k}{\sum_{k=0}^{n} b_k(\omega)^k} \tag{11}$$

This analytical form is fitted numerically to the FRF values obtained in the measurements by selecting appropriate ratios and solving the unknown roots of the polynomials a_k and b_k (Randall et al., 2004), which allows the extraction of frequencies and eigenmodes from the spectrum. The suffix "-Z" refers to the integration of the polynomial method with the mapping of values in the complex plane, which facilitates higher order numerical calculations (Chaun et al., 2007).

Comparison of the obtained vibration forms is possible using the Modal Assurance Criterion (MAC), described in detail in (Kępczak & Witkowski, 2022; Pastor et al., 2007), which is a quantitative indicator of the similarity of modal properties of an object. It is a statistical tool based on the least squares method in determining linear regression. MAC is determined by the normalized scalar product of two sets of vectors, corresponding to the modals being compared. The resulting values are presented in a matrix:

$$MAC(r,q) = \frac{\left|\{\varphi_A\}_r^T\{\varphi_X\}_q\right|^2}{(\{\varphi_A\}_r^T\{\varphi_A\}_r)(\{\varphi_X\}_r^T\{\varphi_X\}_q)} \tag{12}$$

where $\{\varphi_X\}_q$, $\{\varphi_A\}_r$ are the mode shape vectors q and r, $\{\varphi_X\}_q^T\{\varphi_A\}_r^T$ are their transpositions.

In case of complex modes this relation is described by analogous formula:

$$MAC(r,q) = \frac{\left|\{\psi_A\}_r^T\{\psi_X\}_q^*\right|^2}{(\{\psi_A\}_r^T\{\psi_A\}_r^*)(\{\psi_X\}_q^T\{\psi_X\}_q^*)} \tag{13}$$

where $\{\psi_X\}_q\{\psi_A\}_r$ are eigenvectors of complex modes q, r, $\{\psi_X\}_q^T, \{\psi_A\}_r^T$ are their transpositions, and $\{\psi_X\}_q^*$, $\{\psi_A\}_r^*$ are their complex couplings. MAC values are in the 0-1 interval, where 0 means complete independence and 1 means that mode shape pairs exactly match.

AutoMAC is a variant of MAC that focuses on mutual comparison of mode pairs in only one data set. Complete independence in the AutoMAC matrix indicates numerical errors because for an actual test object, the modes should have little dependence on each other, due to the sheer similarity of the object structure and excitation conditions. The MAC table presents the results of calculations in the form of correlation matrix between consecutive pairs of modes from a given set (e.g. a given test).

4. Theory and calculation

4.1. Test object

The test object was the arrangement of the inner wheel and rim of the wheel type 102N, originally used in trams type 13N, 102N, 102Na, 105N, and their derivatives. The materials of which the tested wheel is made, and which were also used in the numerical model, are standardized. Both the disc and the rim are made of carbon steel with increased tensile strength. Especially in the case of the rim, a sufficiently high hardness of the material is important for uniform wear (Piec, 1999). Between the inner disc and the rim there is a press-fit assembly.

Simplifying the structure of the test object by removing additional wheel components, such as damping inserts, bolts and outer discs, allowed the elimination of secondary vibrations that could result from the interaction of parts, which could interfere with the measurement of parameters for the whole object.

The test object is still in use in trams in Polish cities, which introduces the need for more frequent mainte-

nance and repair processes. The analysis of the phenomenon of wear is important not only for diagnostic purposes and traffic safety monitoring, but also to reduce undesirable noise emissions in cities (Komorski et al., 2022). Analysis of dynamic parameters on the test stand and calibration of the modal numerical model with the real one can be a prelude to the development of a methodology for the optimization of the technical condition assessment process also in operational conditions.

4.2. Boundary conditions for numerical analysis

In order to perform the numerical analyses, a 3D model of the object was made in SOLIDWORKS software, which was composed of 76897 finite elements of a high-quality curvature-based solid mesh, and the mesh method was based on the mixed curvature of the model. The mesh model with and gravity load symbol is presented in Fig.1.

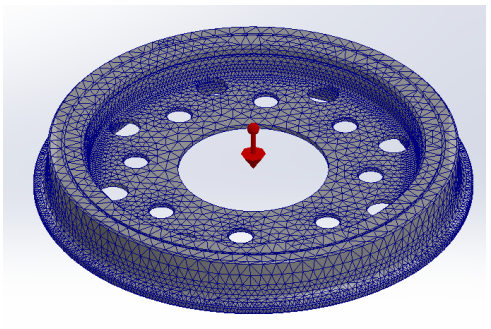

Fig.1. The mesh model with and gravity load symbol of the test object

An accurate representation of the actual object in the CAD environment was made possible by technical documentation and profile measurements using a GRAW A-B type profilometer, with which the geometry of the running and flange surfaces was measured to an accuracy of ±0.1 mm. The material parameters in the simulation were obtained from Polish standards PN-84/H-84027/02 “Steel for railroads - Forgings freely forged – Types” and PN-K-92016 “Tramway wheelsets, flexible - Machined rims - Requirements and tests” for steels used in railroads and uploaded into the material creator in SOLIDWORKS environment. The inner disc material is a structural carbon steel used for free-forged forgings with a designation of P45A, a tensile strength of 600 MPa, a yield strength of 360 MPa and a maximum HB hardness of 220, while the rim material is a steel with a designation of P70, a tensile strength of 1,200 MPa, a yield strength of 700 MPa and a maximum HB hardness of 362.

In Time Response Analysis (also called Modal Time History) the set force is an explicit function of time. This analysis model is used to study short-term phenomena, such as impulsive excitation (Kurowski, 2014). This type of analysis provides displacement and force vectors as a function of time. To determine the modeshapes of an object, the Frequency Analysis tool is dedicated, which does not allow the selection of the location and value of the applied excitation. Thus, it was not applicable to the described study, because it did not allow conditions analogous to the experiment. Therefore, it was decided to analyze dynamic parameters in the processing of signals obtained in the Time Response Analysis.

The boundary conditions of the analysis were intended to represent the main real loads and reactions of the support, and therefore included:

- a gravity load acting vertically with a value of 9.81 m/s^2;
- a stationary restraint with a specified lateral and vertical stiffness of 129 kN/m and a diameter of 330 mm, on which the wheel was supported (simulating the cork spring support used in the experiment);
- an impulse force of 200 N and a duration of 0.01 s (these parameters were estimated from experimental trials).

Due to numerical limitations in the program when determining the boundary conditions in a given analysis, it was decided to not consider the stresses resulting from the push-fit assembly and modeled a common surface contact.

The choice of how and where to simulate the application of an impulse force to the test object model was driven by the conditions of the subsequent experimental study, in which the real object was being subjected to the excitation at the same locations with a modal hammer, while situated on a slightly compressible support. The main concern it was to test the different excitation points in relation to the two measuring points located on the rim and the running surface, in order to obtain the widest range of information on the dynamics of the structure. The force was applied sequentially at points in the outer plane of the rim, according to the designations P1, P2, P3.

The responses were read from points S1 and S2 located on the outer rim plane and the running surface, respectively. The impulse points P1-3 were distant from the transducers S1 and S2 by angular distances of 30º, 90º, and 180º, respectively, relative to the wheel axis. The impulse impact parameters were previously selected based on the analysis of the characteristics of the actual excitation in the experiment. The location diagram of the selected points is shown in Fig.2.

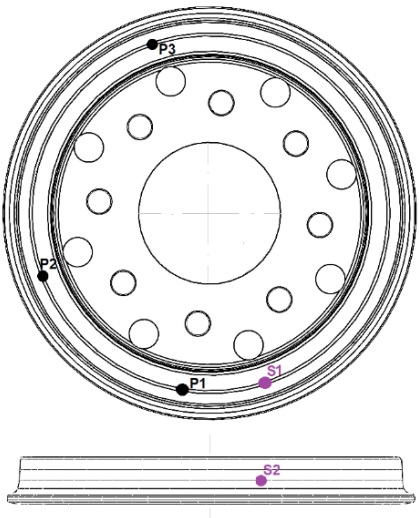

Fig.2. Location of measurement points (S1, S2) and excitation points (P1, P2, P3) on the test object

The damping ratio was expressed as a percentage of critical damping, the value of which was set at 4% in the analysis as assumed for steel structures (Orban, 2010). The entire analysis lasted 1 second, and the expected test frequency range was between 1-3000 Hz. Such range selection was made based on the analysis of running noise tests, which is closely related to the wheel natural frequencies (relevant running noise frequencies are in the range of 200-2000 Hz according to the work (Janssens et al., 2006), and in 100-5000 Hz according to the work (Galaitsis and Bender, 1976).

Time Response analysis was performed using the Direct Sparse solver. The numerical computation of such a system is faster due to optimized data allocation in the computer memory and multi-core and multi-threaded computational processes (Petrova, 2014).

4.3. Test stand

The study of dynamic parameters carried out assumed the use of multiple excitation and measurement points, which is referred to as the MIMO (multiple-input, multiple-output) approach, as it was used to test elements of transport vehicles (Farahani et al., 2018; Milewicz et al., 2022). In order to perform the experimental modal analysis, a modal model was created in the BK Connect software, which allowed to mark the application points of the excitation and the measurement points where the vibration transducers were located. The geometric model consisted of twelve segments, and it considers the rim and flange and reflects the proportions of the real object. The model represented a graphical representation of the object and did not consider the mounting holes of the damping inserts, nor the fasteners in the form of bolts found in the actual wheel, nor the geometry of the running surface. Since the characteristics of the test object are linear, it was possible to decimate the model.

Ten triaxial piezoelectric transducers from Brüel & Kjær were used: four transducers type 4504 A (min. range of measured frequencies is 1 Hz – 11 kHz), three transducers type 4529 B (min. range of measured frequencies is 0.3 Hz – 6 kHz), two transducers type 4524 B (min. range of measured frequencies is 0.25 Hz – 3 kHz) and one single-axis transducer type 4507 B (min. range of measured frequencies is 0.1 Hz – 6 kHz). The expected natural frequencies of the test object were in the range of 1 Hz – 3 kHz, so all transducers met the range and sensitivity requirements.

The transducers were placed, every 120 degrees, on the disc near the hole, on the rim, on the periphery, and two on the running surface. Fig.3A shows a photo of the test object with the transducers already placed, while Fig.3B shows a visualization of the subsequent measurement points in BK Connect, against the model geometry. Points SE1 and SE2 are marked as vibration transducers placed on the rim and running surface, respectively, corresponding to measurement points S1 and S2 in the simulation, while points PE1-3 correspond to points P1-3 in the simulation.

As a local coordinate system, the X-axis was assumed to be radial to the center of the circle, the Y-

axis was assumed to be tangential and clockwise, and the Z-axis was assumed to be vertical with an upward direction (as in Fig. 3B).

Three 12-channel DAQ modules of type Brüel & Kjær 3053-B-12 were used for data acquisition, with a measured frequency range of 0-25.6 kHz. Synchronization of signals in the DAQ modules used was provided by a dedicated switch type PULSE UL-0265. The diagram of the measurement track is shown in Fig. 4.

A modal hammer type Brüel & Kjær 8206-002, with a sensitivity of 2.27 mV/N and a maximum excitation force of 2200 N, was used to perform controlled excitation of the vibration response. An aluminum hammer tip was used, which allowed vibration to be measured over the expected frequency range.

Four repetitions were performed at each of the established excitation points, and the recorded values were then linearly averaged. A total of 40 excitation points were selected, with 9 each on the rim periphery and outer rim plane, 10 on the running surface, and 12 on the inner rim plane. The selection of the points depended on the location of the transducers and the location of the additional holes that are in the actual disc.

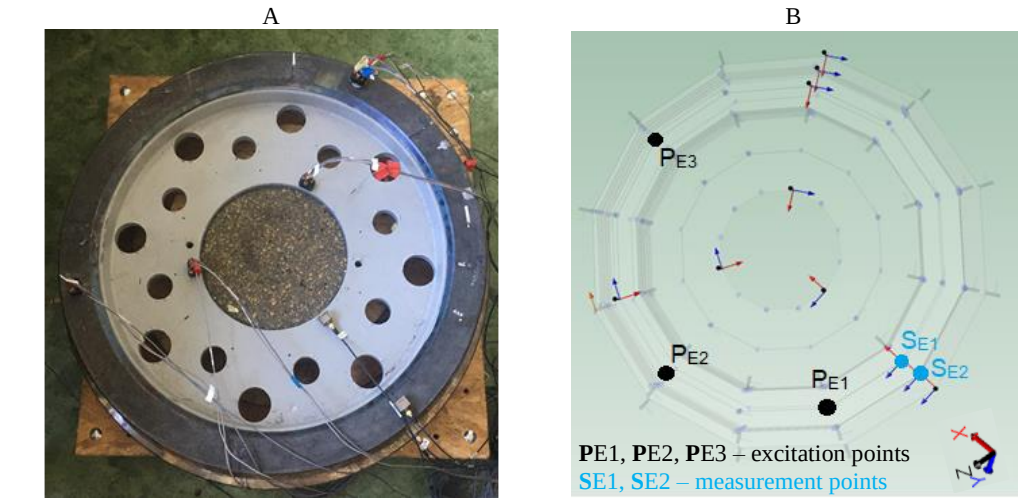

Fig. 3. The real object (A) and its graphic representation (B) with the indication of measurement and excitation points in the experiment, corresponding to points in simulation

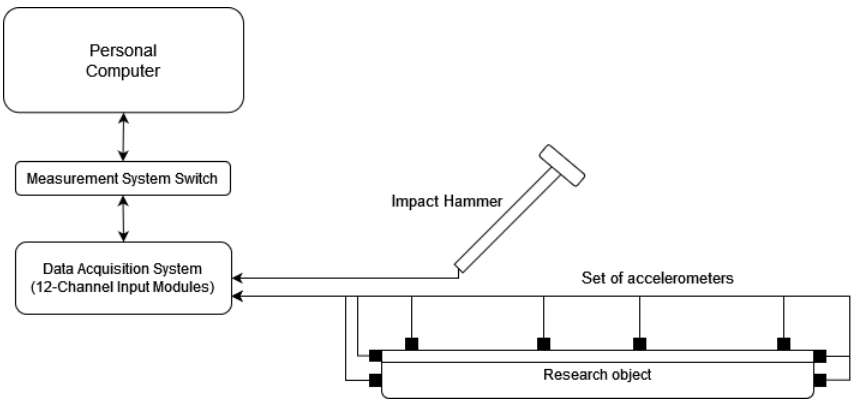

Fig.4. Diagram of the measurement running surface

5. Results

The obtained numerical vectors (vibration acceleration and force) as a function of time were exported from SOLIDWORKS to MATLAB, where they were transformed into frequency responses using the FFT algorithm, to obtain the final FRF. The same number of FFT lines was used as in the experiment, equal to 3200. Fig. 5 shows the characteristics for the excitation points P1-3 and measurement points S1-2. Inertance characteristics show the relationship between the values of the transfer function on the ordinate axis, expressed in units of $(m/s^2)/N$, and the vibration frequency on the cut-off axis (in kHz).

The FRF function analysis identified dominant amplitudes (peaks) whose minimum distance from the lowest contour line was 1 $(m/s^2)/N$. In this way, vectors of location values of the highest vibration acceleration amplitudes were obtained that could be compared with experimentally determined values. In addition, a high-pass filter was applied to reduce the low-frequency modes (<400 Hz) produced only by the numerical calculations. This procedure results from the analyses of the running-frequency tests - in fact, the rails and sleepers are responsible for the measured low-frequency vibrations, while they are not due to the design of the wheel itself (Thompson, 1996).

It can be observed that FRF characteristics are similar for both measuring points, the courses reach local maxima for the same eigenfrequencies, but higher amplitudes correspond to measurements at the wheel rim, which is related to the direction and plane of the applied force. For the excitation at P1, the largest difference between the amplitudes of the corresponding frequency bands is 2.5 $m/s^2/N$, at P2 - 1.5 $m/s^2/N$, and at P3 - 3.5 $m/s^2/N$. Moreover, the FRF values of the dominant bands are higher by 6-10 $m/s^2/N$ for the excitation furthest from the measurement points, compared to the excitations located closer to them (a particularly high difference occurs for bands with frequencies around 1500 Hz). This is probably due to the interference of vibrations at this point since it is located exactly opposite the point of the excitation. The amplitudes peak at 8-12 $m/s^2/N$. The shapes of the spectra change for successive excitation points but are similar for both measurement points. Frequencies in the range 1500-2000 Hz dominate in all of them, while for the higher range the FRF function has noticeably lower values. Three dominant bands for frequencies are duplicated in all six characteristics: 601, 1440 and 1560 Hz.

In the BK environment, the FRF and CMIF functions were calculated analogously. Modes were obtained using the Rational Fraction Polynomial - Z method. This allowed the determination of modal parameters, i.e. eigenfrequencies and damping ratios, and consequently comparison with simulation results. Fig. 6 shows the averaged FRF spectrum considering all measurement points. The resultant amplitude has a different magnitude than the spectra for individual measurement points, because the FRF values are normalized (so when averaging the entire measurement, the amplitude has retained only the proportions).

In contrast, Fig. 7 shows the averaged courses of the vertical vibration acceleration function for all measurement points under the impact force at point No. 1 on the wheel rim, which corresponds to P1 from the simulation. Due to the force excitation in the vertical direction, the expected highest values of vibration acceleration are also achieved for this direction, so we focused on their analysis and interpretation.

The characteristic considering only the vertical component of vibrations for one excitation differs from the one averaged in all directions. The 5 bands of eigenfrequencies are clearly distinguished. In the range 2400-2800 Hz it is possible to notice the absence of two frequencies, so they are related to transverse or radial modes.

On the other hand, Fig. 8 shows the inertance values for the transducers located on the rim and the running surface of the rim (labeled SE1 and SE2 in the experiment according to the schematic in Fig. 3, corresponding to points S1 and S2 in the numerical analysis), under the influence of the excitation on the rim. The force was applied at an angular distance equal to 30º (point PE1), 90º (point PE2) and 180º (point PE3) with respect to the wheel axis, analogous to points P1, P2 and P3 in the simulation.

Three main dominant frequency bands can be observed at 524 Hz, 1436 Hz and 2586 Hz. The other frequency bands correspond to relatively smaller values of vibration acceleration amplitudes. Larger vibration accelerations are achieved at the measuring point located on the running surface (transducer at point SE2), especially for the force applied at the shortest distance (i.e. at PE1) from the values measured on the outer plane of the rim.

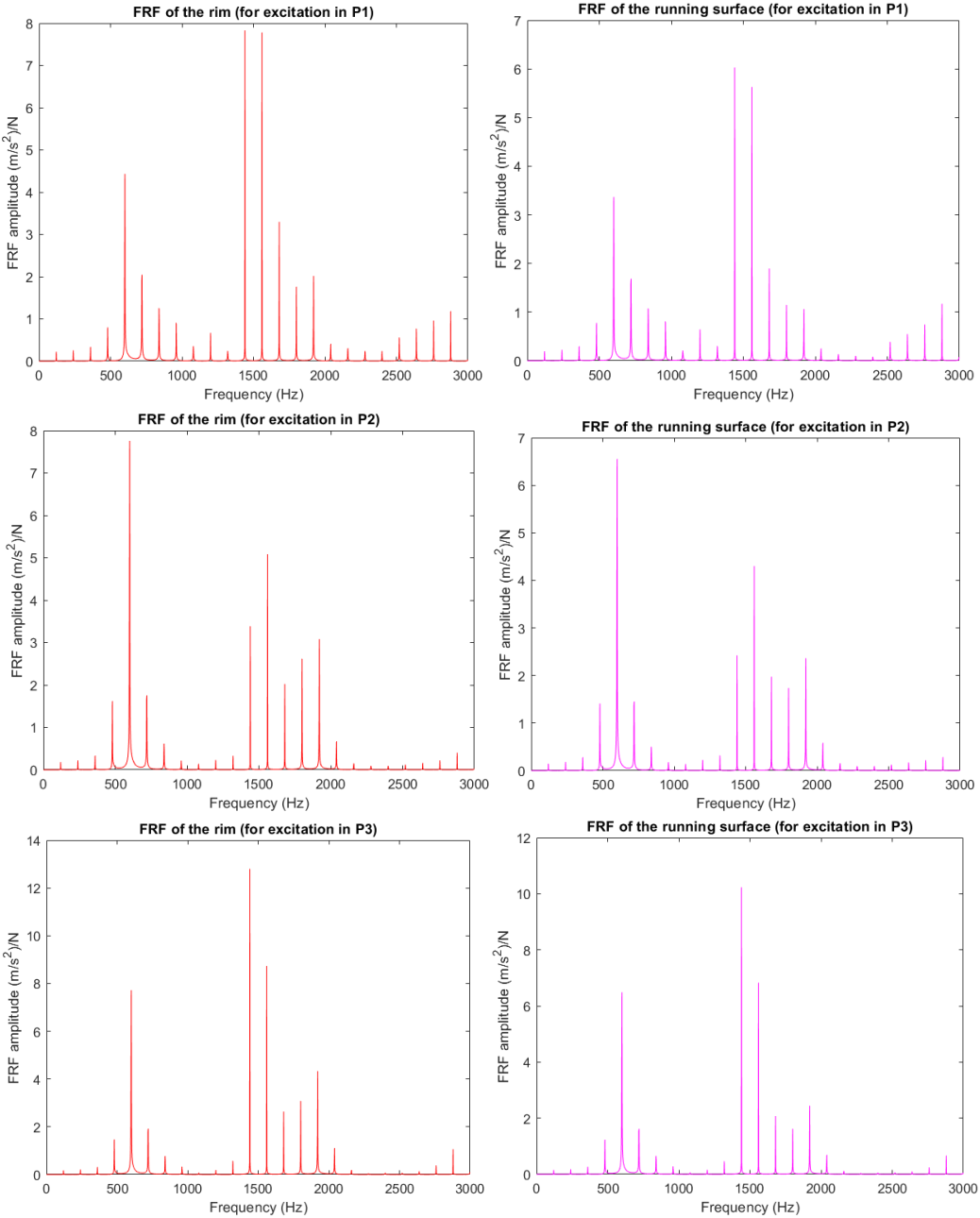

Fig. 5. FRF characteristics of numerical results for rim and running surface for successive excitation points

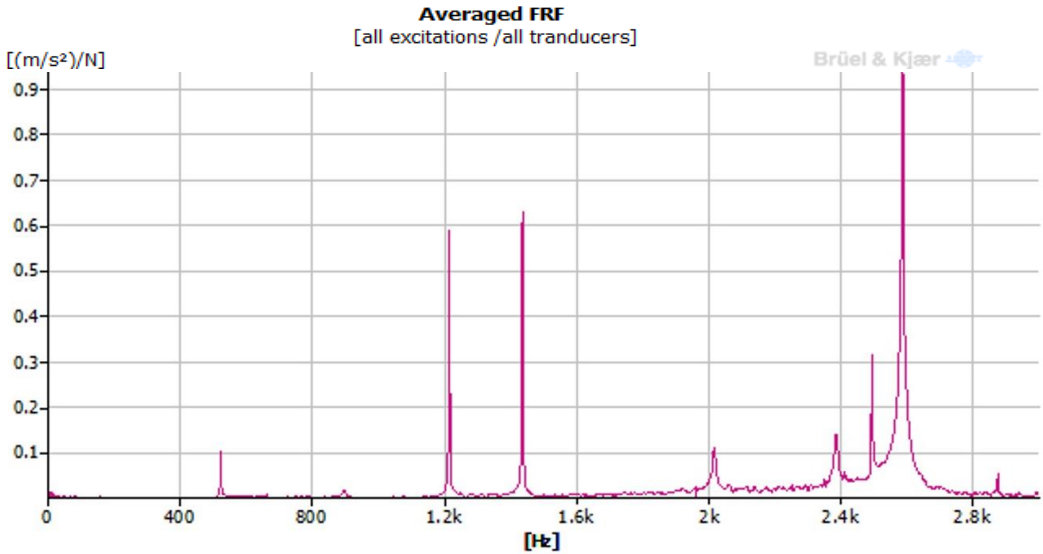

Fig. 6. FRF characteristics averaged over data from all transducers and all excitation points

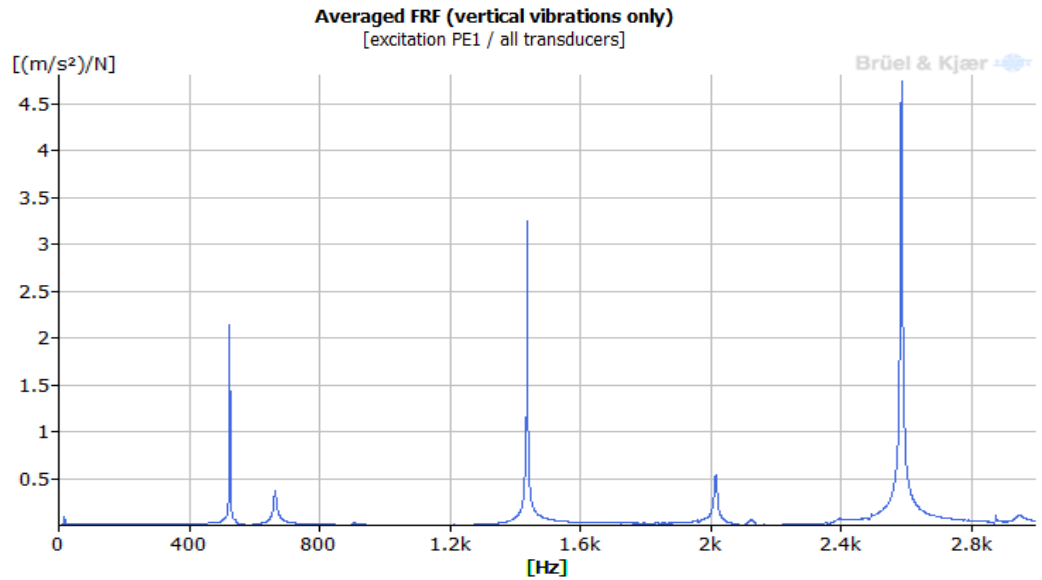

Fig. 7. FRF characteristics in the vertical direction averaged using data from all transducers and the excitation PE1

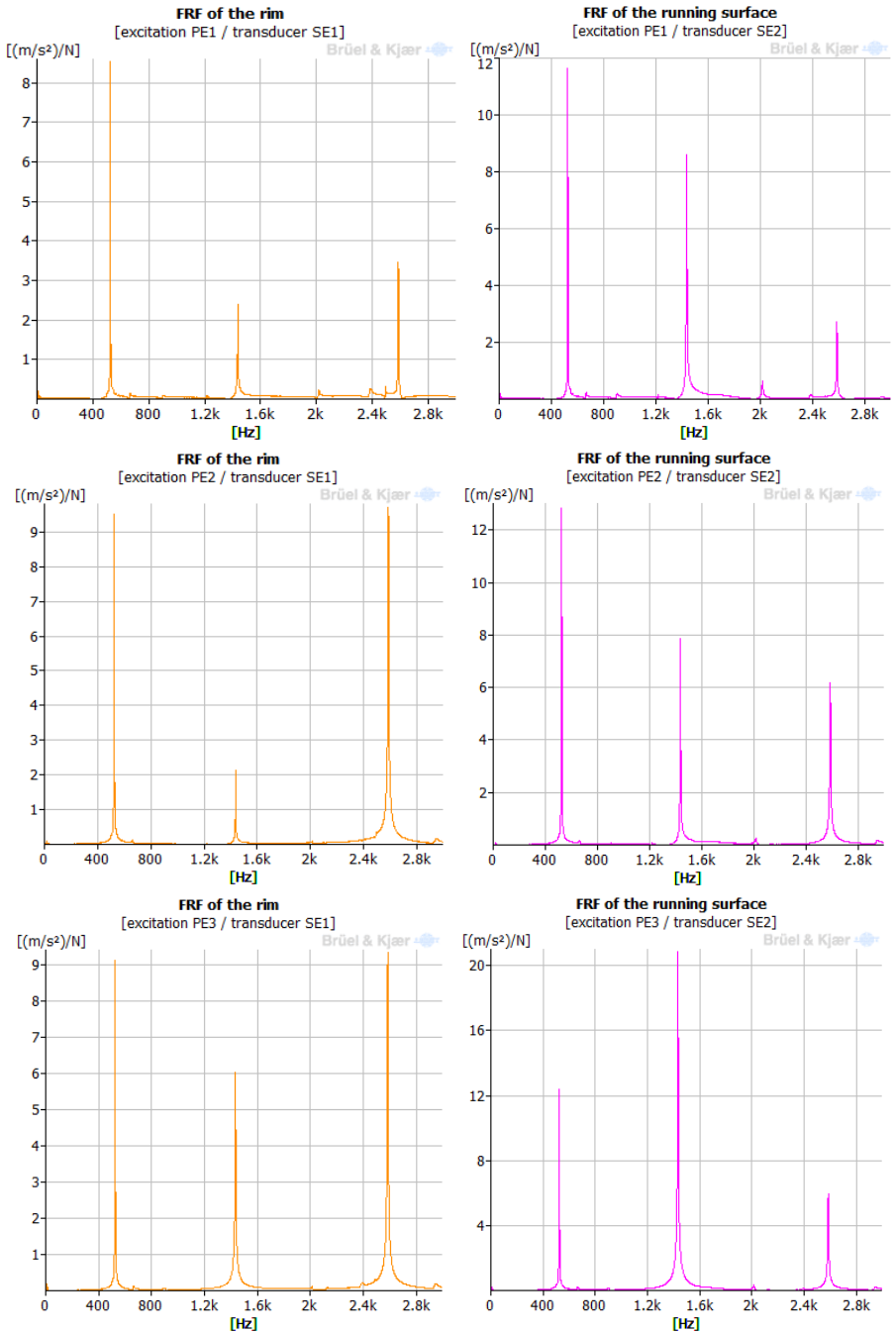

Fig. 8. Characteristics of the inertance measured in SE1 and SE2 to the excitations at successive points (segments) of the rim PE1-3

For SE2, the maximum vibration acceleration amplitude reached a value of 23 m/s²/N for a frequency of 1436 Hz, while the highest value of 8.3 m/s²/N for a frequency of 524 Hz was measured at the rim for the same excitation. In the cases of all three analyzed excitation points, the values of eigenfrequency amplitudes on the inertance characteristics for the rim are at a similar level, not exceeding 10 m/s²/N. However, for measurements at the running surface, noticeably lower amplitudes correspond to the excitation at point PE2 - the highest value is 11.8 Hz at 524 Hz, while the excitation at PE1 and PE3 results in the highest vibration amplitude for the band at 1436 Hz and these values exceed 20 m/s²/N. Fig.9A shows the CMIF diagram for the entire frequency range (and all excitation-response pairs), and Fig.9B shows the selected 400-600 Hz interval. The CMIF function representation is dimensionless and the values are decibel scaled. The obtained default CMIF plot, which shows all the results of the application of this method, contains a lot of information and actually allows a preliminary assessment of the dynamic parameters of the object. Only the analysis of data in narrowed intervals or for selected excitation-response pairs enabled accurate identification of extracted modes and observation of the course of selected functions.

The course of the CMIF function in the selected range shows repeated peaks for each transducer at a frequency of about 524 Hz and identifies the measurement points and vibration measurement directions characterized by the highest amplitude value. In this case, the red and blue curves correspond to the measurement at the very edge of the rim and the measurements in the tangential and radial directions, respectively.

Based on the obtained detailed test results, 6 eigenfrequencies in the investigated range were selected. The selection was made based on:

- FRF and CMIF diagrams, in which the amplitude values were indicative of the occurrence of eigenfrequency,
- results of numerical calculations for selected points of the object,
- the correlation matrix between AutoMAC modes, which made it possible to eliminate duplicate values.

Mode complexity (its high value at low eigenfrequencies indicates possible measurement or processing errors) and damping ratios (which should be low or proportional) were also suggested to reject less reliable analysis results and gross errors.

Table 1 shows the list of eigenfrequencies determined from the analysis of experimental data for selected points and comparison to the results of simulation analysis along with the value of absolute and relative difference. The most convergent values were achieved for frequencies in the middle range - mode III (1436 Hz) and mode IV (2016 Hz). The highest percentage error was obtained for the lowest eigenfrequencies, which is related to the actual damping, probably higher than assumed in the simulation.

The values determined by FRF characteristic analysis for the two selected measurement points and three force application locations were then compared to the modes identified by the RPF-Z method, which uses data for the entire test object. Table 2 shows the resulting eigenfrequencies along with the damping ratio for the identified modes of the object. Proportional damping results in actual modes and oscillation in phase of the degrees of freedom determined in the test (i.e. the nodes of the modal model at which the excitation occurs and the response is measured), while otherwise the modes of eigenfrequency take on an imaginary character and the oscillations are incompatible in phase (Iezzi and Valente, 2017).

High damping occurs mainly at the second lowest eigenfrequencies, while the lowest damping occurs for mode I (524 Hz).

Table 3 shows the AutoMAC cross-correlation matrix for the identified modes, which indicates the mathematical similarities of the eigenfrequency forms. The higher the value in the table, the more similar the correlated modes are in terms of amplitude, location of vibration displacement, and damping.

In all cases, there is no relationship (correlation coefficient less than 0.2) between the selected modes, so the selected eigenmodes have a different character, both in terms of amplitudes and location of areas of enhanced vibrational response. This indicates that the singular properties of the object have been determined, which are neither coupled nor duplicated.

A)

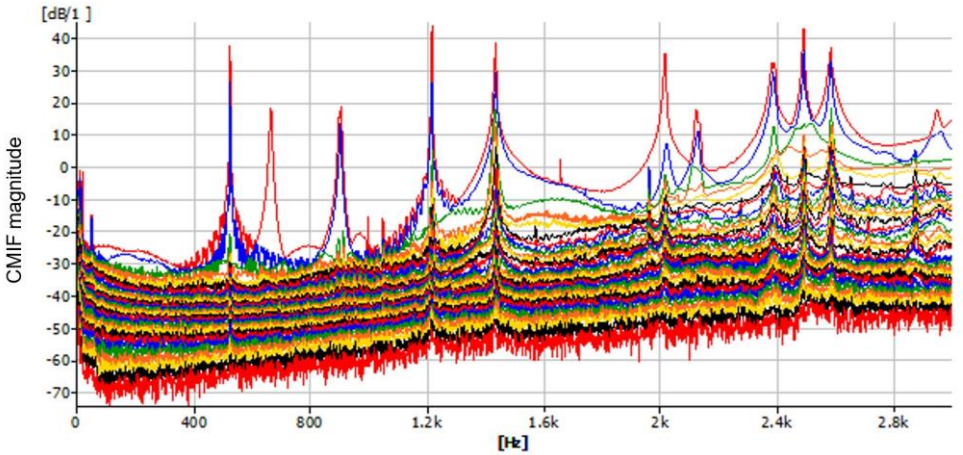

B)

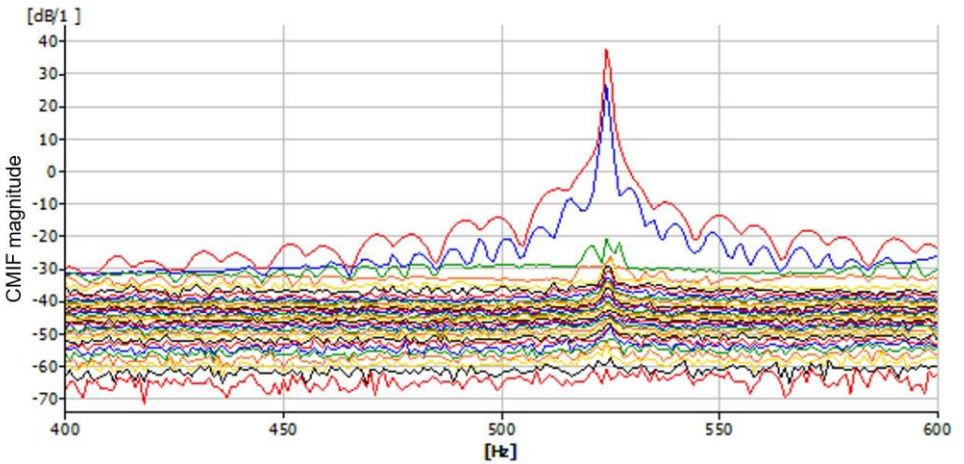

Fig. 9. Diagram of CMIF function for: the whole frequency range tested (A) and 400-600 Hz range (B)

Table 1. Comparison of eigenfrequencies determined from experiment (for selected points) with corresponding numerical results

Mode number	Eigenfrequencies (simulation) [Hz]	Eigenfrequencies (experiment - selected points) [Hz]	Absolute difference [Hz]	Relative difference [%]
I	481	524	43	8.94
II	720	665	55	7.65
III	1440	1436	4	0.28
IV	2040	2016	24	1.23
V	2760	2585	175	6.34
VI	2880	2940	60	2.08

Table 2. Comparison of parameters determined for selected points and for the whole object

Mode number	Eigenfrequencies (experiment - selected points) [Hz]	Eigenfrequencies (experiment - overall) [Hz]	Damping ratio [-]
I	524	524	0.002
II	665	664	0.471
III	1436	1433	0.074
IV	2016	2016	0.172
V	2585	2586	0.093
VI	2940	2948	0.223

Table 3 AutoMAC matrix for the determined forms of eigenfrequency

Hz	524	664	1433	2016	2586	2948
524	1	0.001	0.106	0.011	0.036	0.041
664	0.001	1	0.046	0.003	0.003	0.048
1433	0.106	0.046	1	0.021	0.007	0.015
2016	0.011	0.003	0.021	1	0.046	0.002
2586	0.036	0.003	0.007	0.046	1	0.145
2948	0.041	0.048	0.015	0.002	0.145	1

6. Discussion

Numerical modal analysis resulted in time and FRF characteristics in the range of 1 Hz to 3000 Hz and served mainly as a reference when analyzing the experimental results. The characteristics from the numerical calculations for the points of the structure selected in the analysis under the assumed boundary conditions are close to each other in the shape of the spectrum and the order of the amplitude values. Moreover, only the excitation in the adjacent segment allowed a clear identification of the natural frequencies for the upper part of the range. For the other points, the excitation did not produce significant vertical vibration responses.

However, the theoretical model represents an ideal test situation (with simultaneously limited boundary conditions, estimated material and excitation parameters, also does not consider the actual technical condition of the object), and thus cannot fully represent reality. In order to reliably identify the dynamic parameters of the test object, it was necessary to experimentally determine the values of eigenfrequencies and extract modes from the spectrum, using the CMIF method. It allowed decomposition of FRF values matrix and obtaining information about repeated data, indicating the occurrence of natural vibrations. The experiment also required making a geometric model in BK Connect software and determining its degrees of freedom, as well as its excitation points (locations of modal hammer impacts) and response measurement points (locations of attachment of piezoelectric vibration transducers).

After comparing the data and analyzing the results from both sources, the dynamic parameters that characterize the studied object were finally identified. FRF for selected points of the structure and averaged from all measurement points were used. Experimental and numerical values differed at the extremes by a maximum of 8.9% (1st mode) and a minimum of 0.3% Hz (4th mode) and were characterized by a low damping ratio of no more than 0.5. In the experiment, higher vertical amplitudes were measured with a transducer located on the running surface, in contrast to the simulation analysis, where a stronger vibration response was determined for the outer plane of the rim. This may be related to the elastic support on which the test object was located (causing more damping) or to the compressive forces between the disc and the rim. In addition, the force pulse had one value, determined from previous actual experimental measurements, which may have deviated from the average modal hammer impact value in the experimental study.

AutoMAC matrix correlation analysis determined the relationship between the determined modes of eigenfrequency. For all modes, the correlation values are small enough to be considered singular characters (but greater than zero, so no numerical errors occurred).

The reasons for the differences between the experimental and simulation results may be divided into

those resulting from the measurement method itself, the quality of its execution, numerical limitations and simplification of simulation assumptions. The experimental results, after appropriate selection in the post-processing, can be considered more reliable than the theoretical ones, determined numerically, because of the inclusion of more real factors, high sensitivity of measuring instruments and better computational accuracy in the BK Connect program.

7. Concluding remarks

This paper presents the results of a simulation and experimental study of a tram wheel element system to check the efficiency and calibration capability of the dynamic parameter determination process.

After analyzing the results of the experimental study, six eigenfrequencies were selected, which find their equivalents in the simulation. The eigenfrequencies differ in their damping (except for the lowest frequencies it is relatively low) and in the amplitude of the dominant frequency bands. There were weak cross-correlations in the autocorrelation, indicating that the selected eigenfrequency forms have different characteristics and parameters.

The inertia and CMIF characteristics are a reliable representation of the dynamic susceptibility of the object, which can be used both during construction and retrofit activities. At the design stage, the simulation analysis will allow to obtain information about the ranges of natural frequencies, which are necessary to determine the operating conditions of the object in order to avoid the resonance phenomenon. However, during modernization activities, experimental analysis is applicable. Thanks to comparison of dynamic parameters values before and after given period of exploitation it is possible to identify changes of modal properties, indicating wear or damage propagation. The same effect can be achieved in comparative analysis of theoretical model, determined numerically, calibrated with experimental model. The described study shows the effectiveness of the calibration of these two types of eigenfrequency analysis and can be used to optimize the design, diagnostic and repair processes.

Acknowledgment

The presented results have been co-financed from the subsidies appropriated by the Ministry of Science and Higher Education - 0416/SBAD/0004.

References

[1] Agneni, A., Balis Crema, L., Coppotelli, G. (2010). Output-only analysis of structures with closely spaced poles. *Mechanical Systems and Signal Processing*, *24*, 1240-1249. DOI: 10.1016/j.ymssp.2009.10.013.

[2] Allemang, R., Brown, D. (2006). A Complete Review of the Complex Mode Indicator Function (CMIF) with Applications. *Proceedings of ISMA2006: International Conference on Noise and Vibration Engineering*, *6*.

[3] Amirali, S., Shapou, M. (2021). A new SVD-based filtering technique for operational modal analysis in the presence of harmonic excitation and noise. *Journal of Sound and Vibration*, *510*. DOI: 10.1016/j.jsv.2021.116252.

[4] Bakir, P., Eksioglu, E., Alkan, S.(2012). Reliability analysis of the complex mode indicator function and Hilbert Transform techniques for operational modal analysis. *Expert Systems with Applications*, *39*, 13289–13294. DOI: 10.1016/j.eswa.2012.05.073.

[5] Castillo, M.A., Gutiérrez, R.H.R., Monteiro, U.A., Minette, R.S., Vaz, L.A. (2019). Modal parameters estimation of an electrical submersible pump installed in a test well using numerical and experimental analysis. *Ocean Engineering*, *176*, 1-7. DOI: 10.1016/ j.oceaneng.2019.02.03.

[6] Cataldi-Spinola, E., Glocker, C., Stefanelli, R., Mathias, G. (2004). Eigenfrequency shift of railway wheels due to wear. *Proceedings CFA/DAGA, 04* , 22-26.

[7] Chauhan, S., Martell R., Allemang, R., Brown, D. (2007). Implementation of Complex Frequency Mapping to Low Order Frequency Domain algorithm for Operational Modal Analysis. *Proceedings of the International Modal Analysis Conference*.

[8] Cigada, A., Manzoni, S., Vanali, M. (2008).Vibro-acoustic characterization of railway wheels. *Applied Acoustics*, 69, 530-545. DOI: 10.1016/j.apacoust.2007.01.002.

[9] Cong, S., Hu, S. L. J., Li, H. J. (2022). FRF-based pole-zero method for finite element model updating. *Mechanical Systems and Signal Processing*, *177*, 109206. DOI: 10.1016/j.ymssp.2022.109206.

[10] Eslaminejad, A., Ziejewski, M., Karami, G.

(2019). An experimental–numerical modal analysis for the study of shell-fluid interactions in a clamped hemispherical shell. *Applied Acoustics, 152,* 110-117. DOI: 10.1016/j.apacoust.2019.03.029.

[11] Ewins, D.J. (2000). *Modal Testing: Theory, Practice, and Application*. Research Studies Press, Baldock, 2nd ed.

[12] Farahani, A.M., Mahjoob, M. (2018). Modal Analysis of a Non-rotating Inflated Tire using Experimental and Numerical Methods. *International Journal of Engineering Innovation & Research, 7*, 15-21.

[13] Galaitsis A.G., Bender E.K. (1976). Wheel/rail noise-Part V: Measurement of wheel and rail roughness. *Journal of Sound and Vibration, 46(3),* 437-451. DOI: 10.1016/0022-460X (76)90865-8.

[14] Harak, S.S., Sharma, S.C., Harsha, S.P. (2014). Structural Dynamic Analysis of Freight Railway Wagon Using Finite Element Method. *Procedia Mater Sciencem, 6*, 1891-1898. DOI: 10.1016/j.mspro.2014.07.221.

[15] Hassani, S., Shadan, F. (2022). Using incomplete FRF measurements for damage detection of structures with closely-spaced eigenvalues. *Measurement, 188*, 110388. DOI: 10.1016/j.measurement.2021.110388.

[16] He, J., Fu Z-F. (2001). *Frequency response function measurement*. *Modal Analysis*. Elsevier. DOI: 10.1016/j.proeng.2014.12.136.

[17] Huňady, R., Hagara, M. (2015). Experimental Investigation of Mode Shapes of Symmetric Structures. *Acta Mechanica Slovaca, 19*, 12-17. DOI: 10.21496/ams.2015.018.

[18] Iezzi, F., Valente, C. (2017). Modal Density Influence on Modal Complexity Quantification in Dynamic Systems. *Procedia Engineering, 199*, 942–947. DOI: 10.1016/j.proeng.2017 .09.245.

[19] Jacobsen, N-J. (2018). *Seminar and Workshop on Structural Dynamics*. Poznan University of Technology, Poznan.

[20] Janssens, M.H.A., Dittrich, M.G., Beer, F.G. De, Jones, C.J.C. (2006). Railway noise measurement method for pass-by noise, total effective roughness, transfer functions and track spatial decay. *Journal of Sound and Vibration, 29*, 1007-1028. DOI: 10.1016/j.jsv.2005.08.070.

[21] Kawrza, M., Furtmüller, T., Adam, C. (2022). Experimental and numerical modal analysis of a cross laminated timber floor system in different construction states. *Construction and Building Materials, 344*, 128032. DOI: 10.1016/j.conbuildmat.2022.128032.

[22] Kępczak, N., Witkowski, B. (2022). Modal Assurance Criterion as an iron cast and hybrid machine tool's body comparison tool. *Journal of Manufacturing Processes, 79*, 881-886. DOI: 10.1016/j.jmapro.2022.05.031.

[23] Kim, J. B., Eun, H. C. (2013). Identification of parameter matrices using estimated FRF variation. *Journal of Vibroengineering, 15(1),* 124-131.

[24] Klimenda, F., Soukup, J. (2017). Modal Analysis of Thin Aluminium Plate. *Procedia Engineering,* 177, 11–17. DOI: 10.1016/j.proeng.2017.02.176.

[25] Komorski, P., Nowakowski, T., Firlik, B., Szymanski, G.M. (2018a). Analysis of wheel and track irregularities impact on the vibroacoustic signals emission in rail vehicles. *25th International Congress on Sound and Vibration 2018, ICSV 2018: Hiroshima Calling, 7*, 3864 – 3871.

[26] Komorski, P., Nowakowski, T., Szymanski, G.M., Tomaszewski, F. (2018b). Application of Time-Frequency Analysis of Acoustic Signal to Detecting Flat Places on the Rolling Surface of a Tram Wheel. In: Awrejcewicz, J. (eds) *Dynamical Systems in Applications. DSTA 2017. Springer Proceedings in Mathematics & Statistics, 249*. Springer, Cham. DOI: 10.1007/978-3-319-96601-4_19.

[27] Komorski, P., Szymański, G.M., Nowakowski, T. (2022). Developement of the urban rail vehicle acoustic model. *Applied Acoustic, 195*, DOI: 10.1016/j.apacoust.2022.108807.

[28] Kurowski, P. (2014). *Vibration Analysis with SolidWorks Simulation 2014*, SDC Publications.

[29] Melero, M., Nieto, A. J., Casero-Alonso, V., Palomares, E., Morales, A. L., Ramiro, C., Pintado, P. (2022). Design of Experiments to determine the influence of test procedure on Experimental Modal Analysis. *Journal of Sound and Vibration, 538*, 117229. DOI: 10.1016/j.jsv.2022.117229.

[30] Milewicz J., Mokrzan, D., Szymański, G. M.

(2021). The assessment of the technical condition of SO-3 engine turbine blades using an impulse test. *Combustion Engines, 184*, 24–29. DOI: 10.19206/CE-133872.

[31] Milewicz, J., Mokrzan, D., Nowakowski, T., Szymański, G.M. (2022). Using the MIMO Method to Evaluate the Modal Properties of the Elements of a Wheelset in an Active Experiment. *Vibrations in Physical Systems, 33(3)*, DOI: 10.21008/j.0860-6897.2022.3.24.

[32] Mitchell L. (1982). Improved Methods for the Fast Fourier Transform (FFT) Calculation of the Frequency Response Function. *Journal of Mechanical Design*, *104*, 277–279.

[33] Mokrzan, D., Milewicz, J., Szymański, G.M., Szrama, S. (2021).Vibroacoustic analysis in the assessment of the technical condition of the aircraft airframe composite elements. *Diagnostyka, 22*, 11–20. DOI: 10.29354/diag/135098.

[34] Nadkarni, I., Bhardwaj, R., Ninan, S., Shippa, S.P. (2021). Experimental modal parameter identification and validation of cantilever beam. *Materials Today: Proceedings, 38 (1)*, 319-324. DOI: 10.1016/j.matpr.2020.07.396.

[35] Nangolo, N. F., Soukup, J., Rychlikova, L., Skočilas, J. (2014). A combined numerical and modal analysis on vertical vibration response of railway vehicle. *Procedia Engineering*, *96*, 310-319.

[36] Niziński, S., Michalski, R. (2002). *Diagnostyka obiektów technicznych.* Radom: Instytut Technologii Eksploatacji.

[37] Omar, O., Tounsi, N., Ng, E.G., Elbestawi, M.A. (2010). An optimized rational fraction polynomial approach for modal parameters estimation from FRF measurements. *Journal of mechanical science and technology, 24(3)*, 831-842.

[38] Orban, F. (2010). Damping of materials and members in structures. *Journal of Physics: Conference Series, 268*. DOI: 10.1088/1742-6596/268/1/012022.

[39] Pastor, M., Binda, M., Harčarik, T. (2012). Modal Assurance Criterion. *Procedia Engineering*, 48, 543-548. DOI: 10.1016/j.proeng.2012.09.551.

[40] Pereira, D.A., Guimarães, T.A.M., Resende, H.B., Rade, D.A. (2020). Numerical and experimental analyses of modal frequency and damping in tow-steered CFRP laminates. *Composite Structures*, *244*. DOI: 10.1016/j.compstruct.2020.112190.

[41] Petrova, R.V. (2014). *Introduction to static analysis using SolidWorks simulation*. CRC Press.

[42] Piec, P. (1999). Zjawiska kontaktowe w elementach pojazdów szynowych. *Prace Instytutu Pojazdów Szynowych Politechniki Krakowskiej*, Kraków.

[43] Randall, R., Zurita, G., Wardrop T. (2004). Extraction of modal parameters from response measurements. *Investigación & Desarrollo, 12*, 5–12.

[44] Rao, P. K. V., Varma, G. R. P., Vivek, K. S. (2022). Structural dynamic analysis of freight railway wagon using finite element analysis. *Materials Today: Proceedings, 66(11).* DOI: 10.1016/j.matpr.2022.04.770.

[45] Sowinski, B. (2016). Analysis of high frequency vibration of tram monobloc wheel. *Archives of Transport, 39*, 65-75. DOI:10.5604/08669546.1225450.

[46] Suarez, B., Serrano, B.J., Rodriguez, P., Blanquer, J. (2006). Comparison of Vibration and Rolling Noise Emission of Resilient and Solid Monobloc Railway Wheels in Underground Lines, *Proceedings of the Institution of Mechanical Engineers, 225*, 545-565.

[47] Teimouri-Sichani, M., Ahmadian, H. (2006). Identification of Railway Car Body Model Using Operational Modal Analysis. *Proceedings of the 8th International Railway Transportation Conference (IRTC)*, Tehran.

[48] Thompson D.J. (1996). On the relationship between wheel and rail surface roughness and rolling noise. *Journal of Sound and Vibration*, *193*, 149-160.

[49] Van der Auweraer, H. (2001). Structural dynamics modeling using modal analysis: applications, trends and challenges. *Proceedings of the 18th IEEE Instrumentation and Measurement Technology Conference. Rediscovering Measurement in the Age of Informatics, 3*, 1502-1509. DOI: 10.1109/IMTC.2001.929456.

[50] Wei, L., Sun, Y., Zeng, J., Qu, S. (2022). Experimental and numerical investigation of fatigue failure for metro bogie cowcatchers due

to modal vibration and stress induced by rail corrugation. *Engineering Failure Analysis, 142*, 106810. DOI: 10.1016/j.engfailanal.2022.106810.

[51] Żółtowski, M., Napieraj, K. (2017). Experimental modal analysis in research. *Budownictwo i Architektura, 16 (3)*, 005–012.